Laser Surgery of Port Wine Stains Using Local Vacuum Pressure: Changes in Skin Morphology and Optical Properties (Part I)

Michael A. Childers, MS,[1] Walfre Franco, PhD,[1,2] J. Stuart Nelson, MD, PhD,[2] and Guillermo Aguilar, PhD[1,2]*
[1]*Department of Mechanical Engineering, University of California, Riverside, CA*
[2]*Beckman Laser Institute, University of California, Irvine, CA*

Background and Objectives: In a recent case study, the use of a suction device to aid in port wine stain (PWS) laser treatments showed favorable results. It is our objective to further understand the mechanisms of vacuum-assisted laser therapy by analyzing the mechanical and optical changes of the skin and musculoskeletal tissues during the application of mild vacuum pressure from a suction cup.
Study Design/Materials and Methods: A mathematical model of tissue deformation was used to determine the changes in tissue morphology that affect the underlying laser-tissue interactions, such as epidermal stretching and thinning, blood vessel dilation, and change in blood vessel depth. Video imaging experiments were used to verify the bulk tissue deformation and skin surface stretching computed by the mathematical model. Additionally, visible reflectance spectroscopy was used to determine the changes in the optical characteristics of tissue, including blood vessel dilation and epidermal absorption coefficient.
Results: At a vacuum pressure of 50 kP_a, the epidermis at the center of the suction cup was measured to stretch 4% and was calculated to be thinned approximately 6%. Blood vessels embedded in the dermis were measured to dilate up to two times their original size. However, these vessels were calculated to be displaced toward the skin surface by a very small amount, approximately 1–3 μm. The absorption coefficient of the epidermis was also measured to be reduced significantly by approximately 25% at a wavelength of 585 nm.
Conclusions: Mild vacuum pressure applied to the skin surface causes considerable changes in the morphology and optical properties of the tissue. These changes may be used for more efficient photothermolysis of small PWS blood vessels. Lasers Surg. Med. 39:108–117, 2007.

Key words: port wine stains (PWS); visible reflectance spectra (VRS); blood vessel dilation

INTRODUCTION

Laser-induced photothermolysis (LIP) is currently the preferred method of treatment for port wine stain (PWS) birthmarks, which consist of excessive hypertrophic vessels that give a pink-to-purple coloration to the patient's skin. Unfortunately, PWS are often located on visible anatomic locations, such as face, neck and extremities. During LIP, undesirable blood vessels are heated and photocoagulated by the deposition of laser energy absorbed by blood. While, in general, higher laser doses result in better clinical outcome, the maximum permissible laser dose is often limited by unintentional light absorption and consequent heat generation by epidermal melanin. If laser fluence is not properly adjusted, complications such as hypertrophic scarring, changes in skin pigmentation, atrophy, or induration may occur [1]. To overcome this problem, cryogen spray cooling (CSC) has been utilized [2–4] to pre-cool the skin surface before laser exposure. With the advent of CSC, the clinical outcome of many patients has shown a significant improvement. Dark purple lesions generally fade the most in response to LIP. However, the effectiveness of LIP seems to plateau, resulting in lesions that stabilize at a red–pink color [5].

It is hypothesized herein that the remaining vessels responsible for the red–pink coloration are difficult to destroy due to their small diameters (10–30 μm) [6–8] because smaller vessels have a much lower blood volume-to-vessel wall (perivascular) surface area than larger vessels [9]. This results in insufficient thermal confinement within the vessel and further decreases treatment efficiency. Thus vessels are unable to reach the critical temperature necessary for permanent photocoagulation. In previous studies [10], dilation of these smaller blood vessels using a pressure cuff to obstruct venous blood return showed that an increase in vessel blood volume can reduce the threshold necessary for laser-induced purpura. Subsequent studies [11] using a suction device to impose a local vacuum on the skin surface prior to laser irradiation, further supported the concept of vessel dilation being

Contract grant sponsor: American Society for Laser Medicine and Surgery (A. Ward Ford Research Grant); Contract grant sponsor: National Institutes of Health; Contract grant number: HD-42057.
*Correspondence to: Guillermo Aguilar, PhD, Department of Mechanical Engineering, University of California, Riverside, CA. E-mail: gaguilar@engr.ucr.edu
Accepted 8 October 2006
Published online 26 February 2007 in Wiley InterScience (www.interscience.wiley.com).
DOI 10.1002/lsm.20456

responsible of a more effective vessel microemboli, as evidenced by the more intense purpura following laser irradiation.

The purpose of this work is to analyze and evaluate macro- and microscopic numerical models of the mechanical deformation of human skin and musculoskeletal tissues during the application of local vacuum pressure (P_v) to further understand the physical mechanisms involved. First, a macroscopic (large-scale) model derived from first principles is used to predict the maximum bulk tissue deformation, skin surface stretching, and the epidermal thinning upon the application of mild P_v. The stress-strain field resulting from this model is then used as the initial condition for a microscopic (small-scale) model to predict blood vessel displacement as well as the overall change in blood vessel diameter (D_v) and blood volume fraction (BVF). The results provided by these models are then compared to those gathered using custom-made experimental apparatus. A video imaging system is used to verify bulk tissue deformation and the skin surface stretching. A visible reflectance spectroscope equipped within a vacuum chamber is used to determine the relative change in average D_v and BVF of the dermis as well as the change in the epidermal absorption coefficient ($\mu_{a,e}$) as a function of both P_v and time [12].

NUMERICAL METHODS

Axi-Symmetric Structural Mechanics "Large-Scale Model"

Axi-symmetric structural mechanics equations were solved using the finite element method (FEM) with commercial software (Comsol, Inc., Burlington, MA). The geometry of our large-scale model, shown in Figure 1, consists of two skin layers: epidermis (5×10^{-2} mm thick), dermis (1 mm thick), and musculoskeletal tissue (2×10^{3} mm thick) underneath both skin layers. Due to symmetry, only half of a tissue cross-section of 5×10^{3} mm in diameter is needed for the analysis, as seen in Figure 1.

The tissue along the axis of symmetry is constrained to move only in the axial direction. The bottom and outside (right) boundaries are fully constrained from moving. To simulate the suction cup wall pressing down on the skin, the boundary segment of the skin which makes contact with the suction cup is constrained from moving in its radial direction. The cup is then loaded with a downward pressure which corresponds to the applied P_v. To simulate the application of P_v, a vertical upward pressure is homogeneously applied over the skin surface area within the suction cup.

In order to analyze the solution to the numerical model, the skin geometry in the area of applied pressure is divided into five different regions, each 3 mm in length, as illustrated in Figure 1. Region 1 is the innermost region, closest to the axis of symmetry, while Region 5 is the outermost region closest to the suction cup wall.

The axi-symmetric structural mechanics equations are a transformation of the stress/strain equations from rectangular (x, y, and z) into cylindrical coordinates (r, z, and φ). Normal strain is defined as the elongation or contraction of a line segment per unit length, while shear strain is defined as the change in angle that occurs between two line segments which are originally perpendicular to each other. In cylindrical coordinates, the three normal strain components (ε_r, ε_z, ε_φ) and the shear strain (ε_{rz}) are given as,

$$\varepsilon_r = \frac{\partial u}{\partial r}, \quad \varepsilon_z = \frac{\partial w}{\partial z}, \quad \varepsilon_\varphi = \frac{u}{r}, \quad \varepsilon_{rz} = \frac{1}{2}\left(\frac{\partial u}{\partial z} + \frac{\partial w}{\partial r}\right) \tag{1}$$

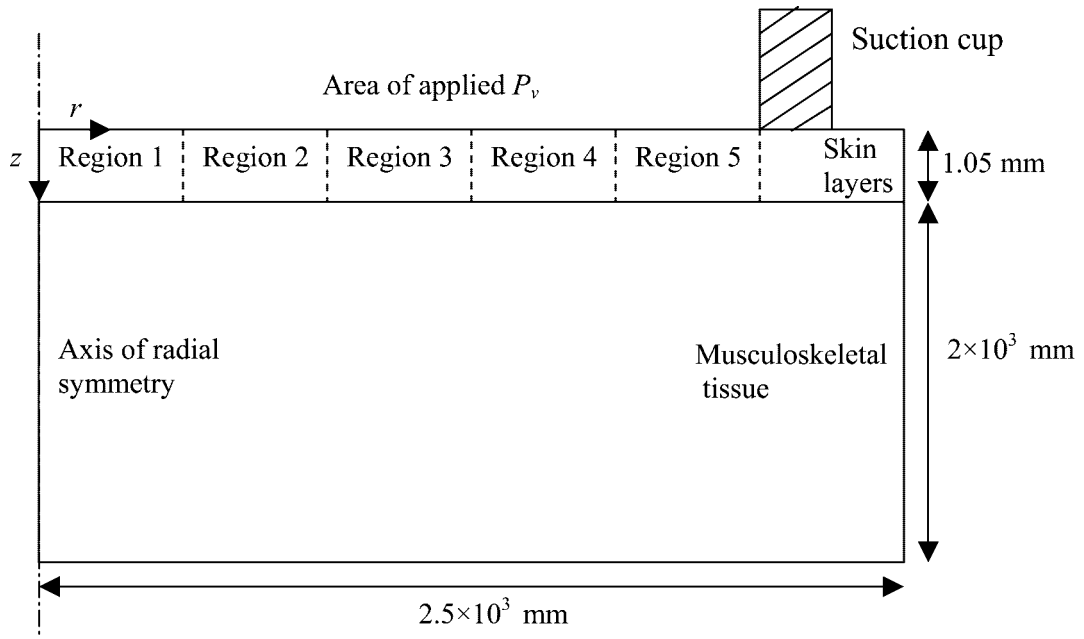

Fig. 1. Large-scale model cross sectional geometry.

where u and w are the displacement components in the radial and vertical directions, respectively. For materials that exhibit a linear relationship between stress and strain, Hooke's law may be used to represent the stress of a material as a function of mechanical strain. Hooke's law simply states that stress is directly proportional to strain, where the modulus of elasticity (E) is the proportionality constant. In cylindrical coordinates, Hooke's law can be represented as,

$$\sigma_{ij} = \lambda \varepsilon_{mm} \delta_{ij} + 2\mu \varepsilon_{ij} \tag{2}$$

where σ_r, σ_z, and σ_φ are the normal stress components, σ_{rz} is the shear stress component, ε_r, ε_z, and ε_φ are the normal strain components, ε_{rz} is the shear strain component, and λ and μ are Lame's constants, defined as

$$\lambda = \frac{2\mu v}{(1-2v)} \quad \mu = \frac{E}{2(1+v)}, \tag{3}$$

In order to solve for global displacement (u, w) using the stress/strain equations, the following set of equilibrium equations were used to describe stress of the system in terms of the volume, or body, forces acting on it,

$$\frac{\partial \sigma_r}{\partial r} + \frac{\partial \sigma_{rz}}{\partial z} + \frac{\sigma_r - \sigma_\varphi}{r} + K_r = 0, \quad \frac{\partial \sigma_{rz}}{\partial r} + \frac{\partial \sigma_z}{\partial z} + \frac{\sigma_{rz}}{r} + K_z = 0, \tag{4}$$

where σ_r, σ_z, and σ_φ are the normal stress components, σ_{rz} is the shear stress component, and K_r and K_z are the volume force (body force) components.

It should be noted that, for the derivation of these structural mechanics equations, it must be assumed that the material being modeled is a homogeneous, isotropic, and linearly elastic. Skin, however, has been clearly documented and observed to be a non-linear elastic material. This non-linear stress-strain relationship is a result of the non-homogeneous composition of human skin. Skin structure is composed of a network of different protein fibers, of which the most prominent and strongest are collagen fibers [13] which run parallel with the skin surface in wavy coils. Elastin fibers are the second most prominent component found in the dermis. These fibers have a much lower stiffness than that of collagen and can stretch up to 100% of their initial length [14]. The non-linear stress-strain relation of skin can be seen in the stress-strain curve shown in Figure 2 and can be characterized into three distinct stages. In the first stage, collagen fibers start to uncoil and align in the direction of strain while elastin fibers contribute to the majority of the resistance to stretching. During this stage, the stress-strain relationship is approximately linear and has a constant elastic modulus.

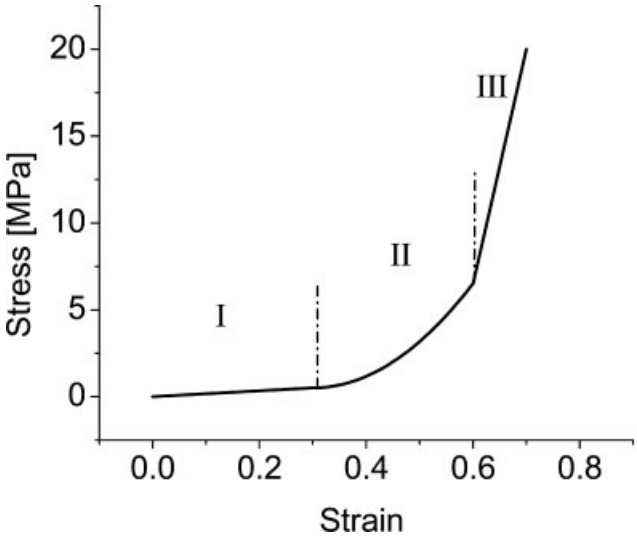

Fig. 2. Non-linear stress-strain diagram for human skin from [15].

However, in the second stage, collagen fibers start to become fully uncoiled and the skin slowly becomes stiffer. Finally, in the third stage, all of the collagen fibers become unwound and exert the majority of skin resistance [15].

Because of this non-linear elastic relationship, our model is limited to strains that keep the tissue within the first stage of the stress-strain curve (i.e., linear region). Pressures that cause stresses to exceed this stage will result in an increasing deviation from the linear relationship. The material properties used for our model are summarized in Table 1 [13,14,16,17].

Axi-Symmetric Structural Mechanics "Small-Scale Model"

To further understand the mechanical effects of the application of P_v from a suction cup on the microstructures of skin, a small-scale model of tissue deformation was developed. The model geometry, shown in Figure 3, was chosen to be identical to the skin layer regions assigned in the macroscopic model (3 mm$\times$1.05 mm) and consisted of the epidermis, represented by the top layer; the dermis, represented by the bottom layer, and an embedded blood vessel of diameter D_v, vessel wall thickness t, at depth Z. The top boundary of the geometry was loaded with an upward vertical pressure, P_v and the two sides of the region were loaded with a corresponding pressure gradient calculated from the large-scale model. The bottom boundary of

TABLE 1. Material Properties of Human Tissues [13,14,16,17]

	Perivascular Tissue	Epidermis	Dermis	Musculoskeletal
Elastic Modulus (Mpa)	1.23	0.5	2	0.56
Poisson's Ratio	0.3	0.3	0.33	0.27
Density (kg/m^3)	1056	1110	1116	1038

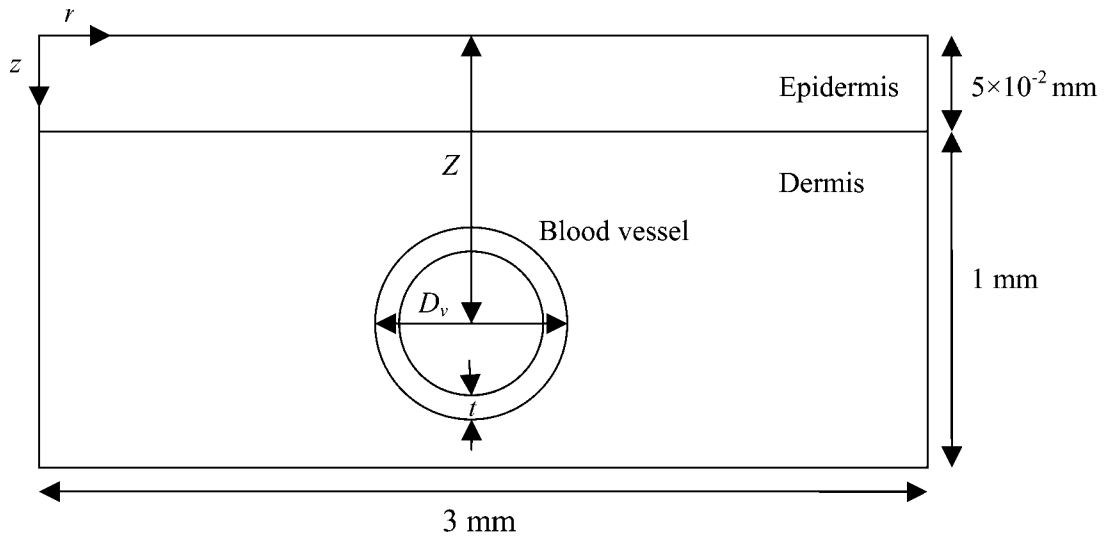

Fig. 3. Small-scale model cross-sectional geometry.

the geometry was then constrained in both the axial and vertical directions. By constraining the bottom boundary, the dermis is unable to bow. Although this constraint may be too restrictive and unsupported by actual experimental evidence, only a small underestimation (~6%) of tissue deformation was observed in Region 1 of the small-scale model when compared with the large-scale model because the curvature in the region at the center of the suction cup is very small.

EXPERIMENTAL METHODS

Displacement Video Imaging

To verify the results generated from the numerical model, a set of video-based experiments were conducted to show the displacement and stretching of the bulk tissue under P_v. A high speed CCD video camera was directed perpendicular to the axis of the suction cup in the same horizontal plane that the skin surface contacts the cup. A vacuum pump was then connected to the cup in order to apply the required amount of suction. Using this setup, the maximum vertical skin displacement at the center of the suction cup can be imaged and compared to the maximum vertical displacement calculated by the large-scale numerical model. In order to verify the stretching, six parallel lines were drawn on a volunteer's skin surface 3 mm apart from each other, as shown in Figure 4. These lines divide the skin into five regions corresponding to those of the numerical model which were imaged before (Fig. 4A) and after (Fig. 4B) application of P_v. Using commercially available video analysis software (Photron Motion Tools, Photron USA, Inc., San Diego, CA), the change in distance between the lines was calculated to determine the amount of stretching that occurred at the skin surface for a given P_v.

Visible Reflectance Spectroscopy (VRS)

VRS is a non-invasive technique widely used to determine the chromophores present within human skin [18–20]. Of all skin chromophores, melanin and hemoglobin are the two predominant absorbers within the visible light spectrum. Epidermal melanin absorption decreases monotonically from the ultraviolet to the infrared range, thus causing a steady increase in the reflectance spectra of human skin towards longer wavelengths [12]. Oxyhemoglobin absorbs strongly in the 500–600 nm range and is responsible for a set of dips in the reflectance spectra at 542 and 577 nm. In the near infrared (700–900 nm) deoxyhemoglobin absorbs strongest at 760 nm, which can also be seen as a dip in the spectra at that wavelength. These optical characteristics of human skin have been reconstructed from the VRS measurements using an optical diffusion approximation of a multilayer analytical model [21,22] which can be used to fit measured reflectance spectra by varying the optical parameters of each layer within the model [23].

In summary, this model consists of two homogeneous layers of uniform thickness: the first composed of epidermis and papillary dermis and the second of the deeper dermis. Each layer is represented by absorption, scattering and anisotropy coefficients (μ_a, μ_s, and g, respectively) as mathematical expressions dependent on wavelength (λ)

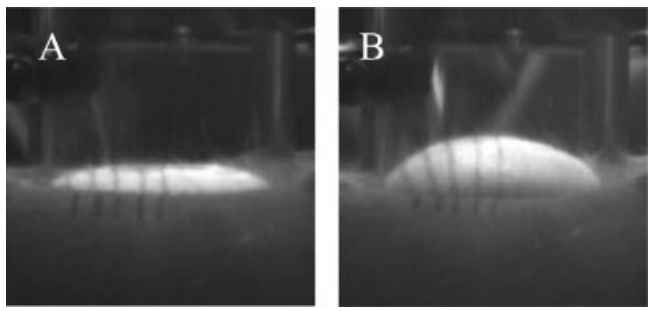

Fig. 4. Images of skin regions (**A**) before and (**B**) after the application of $P_v = 50\ kP_a$.

and weighted averages dependent on the concentration of blood and melanin in each layer. Therefore, for the spectral range of 400–800 nm (covered by the VRS), one set of composite optical properties μ_a, μ_s, and g are required for the epidermal ($\mu_{a,e}$, $\mu_{s,e}$, and g_e) and dermal layers ($\mu_{a,d}$, $\mu_{s,d}$, and g_d), which are dependent on the BVF, melanin concentration (epidermis only), hematocrit and average vessel diameter (D_v).

For this study, we fixed the epidermal/papillary dermis thickness at 50 μm and the deeper dermis at 1 mm and assumed a fair skin patient (type II) with a melanin concentration of 7%; hematocrit was kept at 0.41 and the initial BVF of the epidermal/papillary dermis layer and deeper dermis was set at 0.2% and 1%, respectively, in accordance with Svaasand et al. [10].

Using VRS and this model, a set of experiments were developed to determine the change in skin optical characteristics under atmospheric and vacuum pressures. A vacuum chamber, seen in Figure 5, was built with the same diameter opening as the suction cup. Inside the chamber, an ISP-REF integrating sphere with a built-in broad spectrum white light source fitted to an Ocean Optics SD2000 spectrometer was placed (Fig. 5). The integrating sphere-spectrometer arrangement was calibrated using a WS-1 diffuse reflectance standard and a low-reflectivity specular reflectance standard before each set of experiments. The vacuum chamber was designed to enable skin deformation caused by suction while maintaining the integrating sphere in contact with the skin at all times, thus allowing the capture of real-time total spectra before, during, and after application of P_v. From the resulting spectra, the diffusion approximation model was then used to determine the change in dermal BVF and $\mu_{a,e}$ as a function of both P_v and time. All measurements done on subjects were carried out at room temperature with the volunteers in a resting or inactive state for at least 20 minutes prior to experimentation. This controlled environment helped to minimize changes caused by known physiological responses to stimuli such as ambient temperature and activity of the subject.

RESULTS

Axi-Symmetric "Large-Scale Model" and Displacement Video Imaging

As evident in Figure 6A,B, skin displacement measured by the video imaging apparatus (Fig. 6A) was reasonably well predicted by the large-scale numerical model (Fig. 6B). In Figure 7A, the maximum displacement at the center of the suction cup calculated by the large-scale model (solid line), showed a linear relationship with P_v. This prediction agreed well with the measured displacement at the center of the suction cup (symbols) confirming the linear relationship between displacement and P_v up to about $P_v = 34$ kP_a. Note, however, that once P_v goes higher than this value, the experimental data begins to level.

Figure 7B shows both the large-scale model predictions (lines) and video imaging results (symbols) of the skin surface stretching for all five regions as a function of P_v. Note that the stretching of the skin surface occurs mostly in the outer regions near the suction cup wall.

Finally, the large-scale numerical model was also used to compute the extent of epidermal thinning. Figure 8 showed that the epidermis was thinned by a relatively small amount ($\leq$6%) due to the application of P_v for the first four regions.

Axi-Symmetric "Small-Scale Model"

Figure 9 shows displacement of a simulated small blood vessel embedded within the dermis as a function of P_v. At the maximum P_v (50 kP_a), vessels are only displaced approximately 2.5 μm toward the skin surface relative to their position at P_{atm}. Similarly, Figure 10A (dotted line) shows that D_v increases from 10.7 μm at P_{atm} to 11.2 μm at $P_v = 50$ kP_a according to the model predictions, which corresponds to a mere 0.3% increase in the BVF of tissue

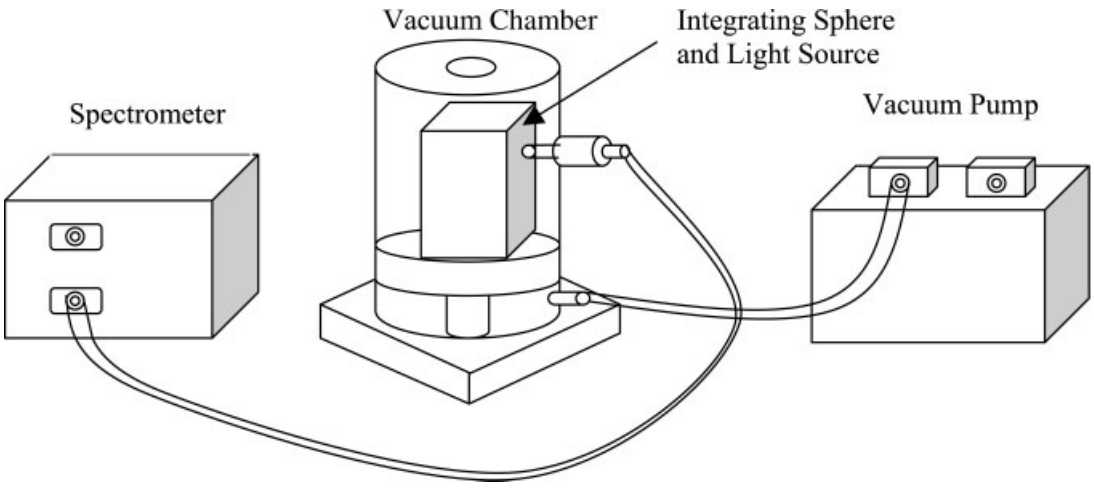

Fig. 5. Spectrometer experimental setup.

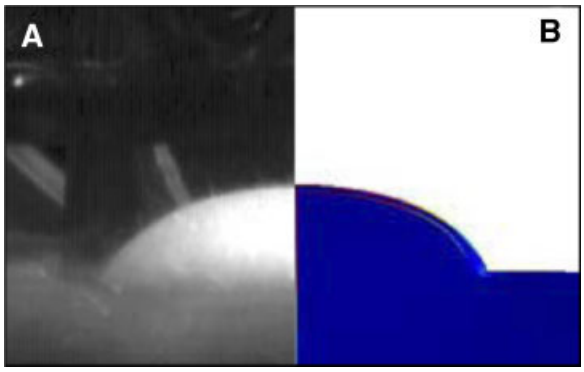

Fig. 6. **A**: Image of bulk tissue deformation on forearm of subject exposed to $P_v = 34$ kP_a of vacuum pressure; (**B**) skin deformation computed by structural mechanics model at same P_v.

(solid line). These results suggest that both vessel displacement and dilation are minimal due to mechanical effects alone.

Visible Reflectance Spectroscopy (VRS)

Figure 10A also shows BVF (squares) and average D_v (triangles) as measured by VRS and computed by the diffusion approximation model [21], plotted as a function of P_v. Based on these indirect measurements, blood vessels dilate significantly more than that calculated by the small-scale numerical model. This figure also shows that BVF and average D_v increase non-linearly with applied P_v and have much steeper slopes for lower P_v than at larger P_v.

The change in BVF and D_v as a function of time can be seen in Figure 10B where there is a short period of time in which the skin undergoes a reduction in BVF and D_v. This blanching effect occurs during the first half second of applied P_v, when the bulk tissue is still being deformed by the suction. Beyond this time period, BVF increases by approximately 10% corresponding to an approximately twofold increase in D_v.

The skin optical characteristics are also changed by application of P_v by the suction cup. In Figure 11A, the change in $\mu_{a,e}$ is plotted as a function of P_v. It can be seen that $\mu_{a,e}$ decreases approximately linearly with P_v. The time scale required for this change can be seen in Figure 11B, where most of the change in $\mu_{a,e}$ occurs within

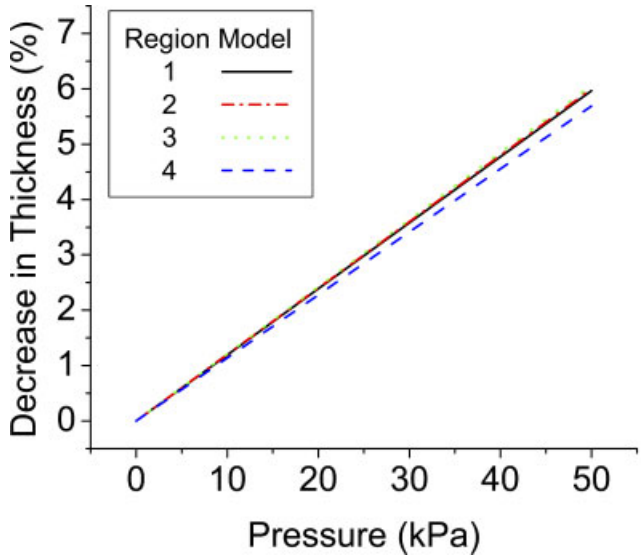

Fig. 8. Large-scale numerical model results: thinning of the epidermis by applied P_v.

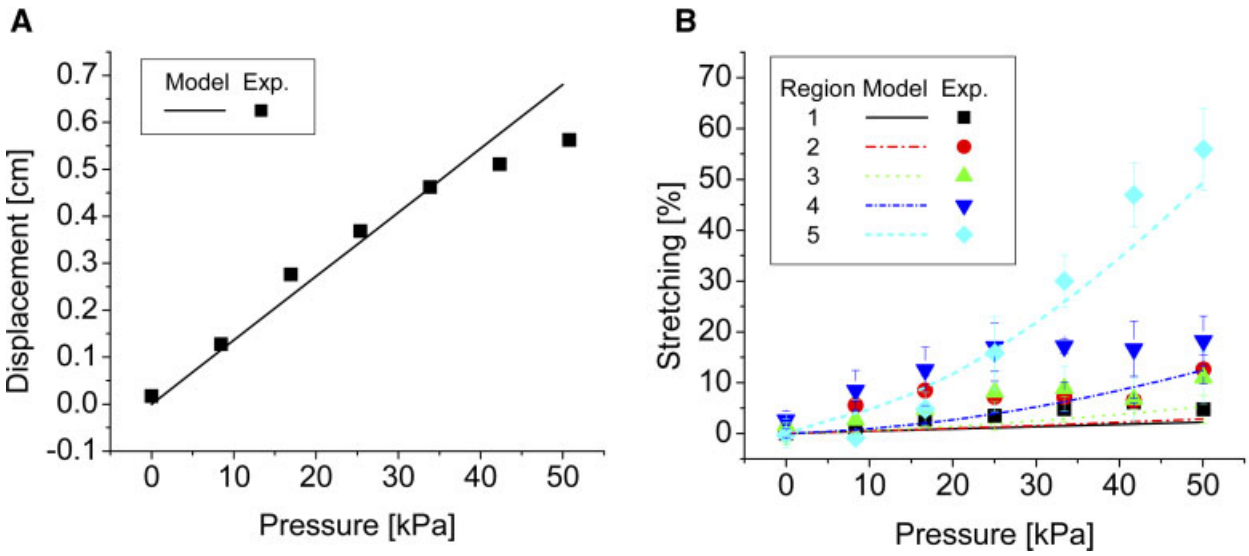

Fig. 7. Large-scale numerical model and displacement video imaging results: (**A**) maximum vertical displacement of tissue at center of suction cup by applied P_v; (**B**) regional surface stretching of skin versus applied P_v. Error bars denote standard deviations of 3–5 experiments at every given pressure.

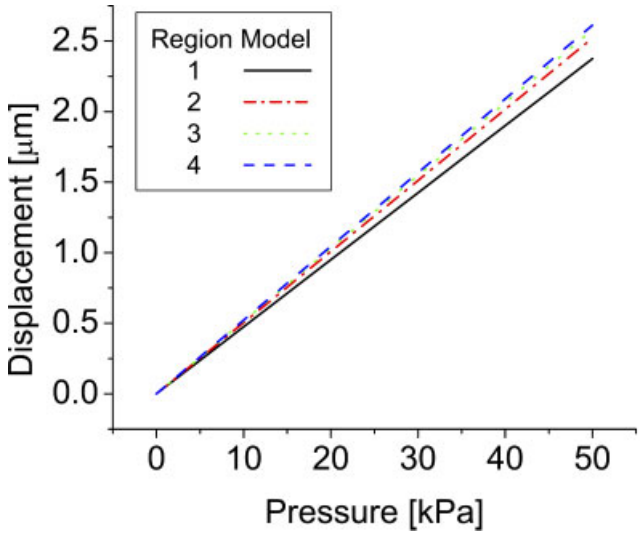

Fig. 9. Small-scale numerical model results: vein to surface displacement of a blood vessel at a depth of 250 μm by applied P_v.

the first second of applied P_v, corresponding approximately to the time when bulk tissue deformation occurs.

DISCUSSION

The leveling off of the experimental data for the maximum displacement at the center of the suction cup, as seen in Figure 7A, corresponds to the stress at which the tissue reaches the transitional or second stage of the non-linear stress-strain relationship shown in Figure 2. This is further supported by the surface stretching of the skin seen for each region (Fig. 7B). As Region 5 reaches approximately $P_v = 34$ kP_a, tissue in that region starts to transition from the linear to non-linear stress-strain relationship, which leads to inaccuracies within the large-scale model. It should be noted that the errors seen in the regions away from the suction cup wall, particularly Region 1, are much smaller since the strain in these regions does not exceed the linear to non-linear transition (strain ~0.3).

Application of P_v from a suction cup not only stretches the skin but also induces changes in the epidermal thickness. Hendriks et al. [24] measured in vivo a 7% and 17% reduction in human skin thickness composites (epidermis and papillary dermis) at 20 and 35 kP_a suction pressures, respectively. Our model predicted a 6.5% reduction in epidermal thickness under $P_v = 50$ kP_a. It is logical to conclude that a reduced epidermal thickness would result in more light being delivered to sub-epidermal structures because of potential increments in light transmittance. Moreover, the skin surface roughness is also altered by P_v from the suction cup, rendering a smooth surface for which changes in light reflectance are also expected [25].

Results from the numerical modeling show that blood vessels are displaced toward the skin surface only 2.5 μm at $P_v = 50$ kP_a (Fig. 9). Such a small vertical displacement of a vessel should not have a significant impact on light deposition and, consequently, heat diffusion [9].

The BVF and vessel dilation measured by VRS experiments were much greater then the values calculated by the small-scale numerical model (Fig. 10A). In addition, the time calculated for the change in BVF and D_v was much greater than the elapsed time of bulk tissue deformation (Fig. 10B). This is because the increase in D_v in the dermis is not simply the result of applied mechanical forces alone, but is more likely due to the body's physiological response to locally applied pressure. Vessel constriction and dilation control are essential for the body's circulatory system to properly function. Generally, circulation adjustments are produced by changing the cardiac output, the amount of

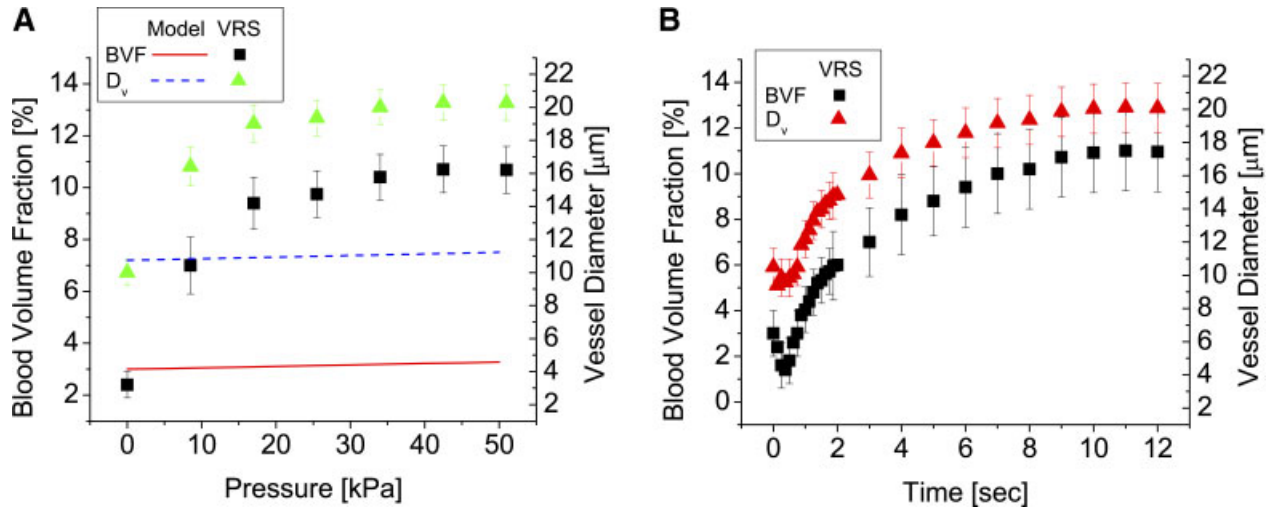

Fig. 10. Small-scale numerical model and VRS results: (**A**) changes in BVF and average D_v as a function of applied P_v on the forearm of a 24-year-old male with type II skin; (**B**) changes in BVF and average D_v as a function of time with the application of $P_v = 50$ kP_a on the palm of a 24-year-old male.

resistance produced by the arterioles, and by varying the amount of blood that is pooled within the venules [26]. The size of the arterioles and venules located within the skin are controlled in part by the body's systemic mechanisms, but are also effected by local regulatory mechanisms. The systemic regulation of vessels is governed by vasoactive substances secreted by the body and by vasomotor nerves that innervate the arteriole's smooth muscle. However, localized control of arterioles and venules are managed mainly by vasodilator metabolites secreted by surrounding tissue. One such tissue which can release these vasodilator metabolites are endothelium cells (EC) [27] which are part of the blood vessel and are located between the circulating blood and the media and adventitia of the blood vessel wall. The EC respond to many different stimuli including flow changes, stretching, shear stress, and a variety of substances circulating throughout the blood stream. One such substance secreted by the EC that is crucial to vasodilatation is Endothelium-Derived Relaxing Factor (EDRF) or nitric oxide. EDRF acts directly on smooth vascular muscle tissue to relax cells and allow vasodilatation. The release of EDRF is triggered by the presence of acetylcholine and bradykine within the blood stream or by shear stress in the cell wall.

When suction is applied to a localized region on the skin surface, the EC within vessel walls are exposed to mechanical strain and stress. As a result, EDRF is released and the smooth muscle tissue of the blood vessels is relaxed. In Figure 10B, the BVF and D_v changes of tissue recorded increased more rapidly at lower than larger P_v. It would appear that at lower P_v the increase in BVF and D_v is driven predominately by muscle relaxation. However, once smooth muscles have fully relaxed, the rate of increases in BVF and D_v with pressure are reduced and likely further driven by the mechanical strain applied to the vessel walls.

Stretching and compression of human skin alters its optical properties [28]. Jacques et al. [29] reported a reduction in the volumetric fraction of melanosomes proportional to the reduction in epidermal thickness; that is a 23% reduction at 2.4 kP_a suction pressure (which seems too small of a suction pressure for such a reduction, perhaps a typographical error in the reported value of pressure). Chan et al. [30] measured in vitro changes in optical properties of pig and human skin slabs as a function of compression load; there was an increase in transmittance, absorption, and scattering coefficients and a reduction in reflectance among most of the compressed specimens which the authors attributed the effects to changes in shape of cellular components, reduction in index-mismatch and changes in scatterer and chromophore concentrations. As the VRS results show in Figure 11, there were significant reductions in $\mu_{a,e}$ observed from the application of P_v. This is attributed to the thinning and stretching of the epidermis which alters the spatial distribution of melanin, thus reducing its concentration per unit area.

During the application of P_v with the suction cup, it is observed that a local erythema develops (i.e., local BVF increases) similar to that reported by Svaasand et al. [10] during the obstruction of the venous return of the upper extremity of one subject. This increase in BVF was accompanied by a reduction of the reflectivity over the entire spectrum (Fig. 1, Svaasand et al. [10]). However, it was also noted in that article that the two characteristic oxyhemoglobin absorption peaks at 542 and 577 nm disappeared after 3 minutes of venous blood obstruction, while the characteristic de-oxyhemoglobin peak at 760 nm increased, indicating blood de-oxygenation.

Figure 12 shows the change in the reflectance spectra at 1 and 10 seconds after $P_v = 50$ kP_a is applied to the forearm of a fair skin subject (type II). Note that while an overall

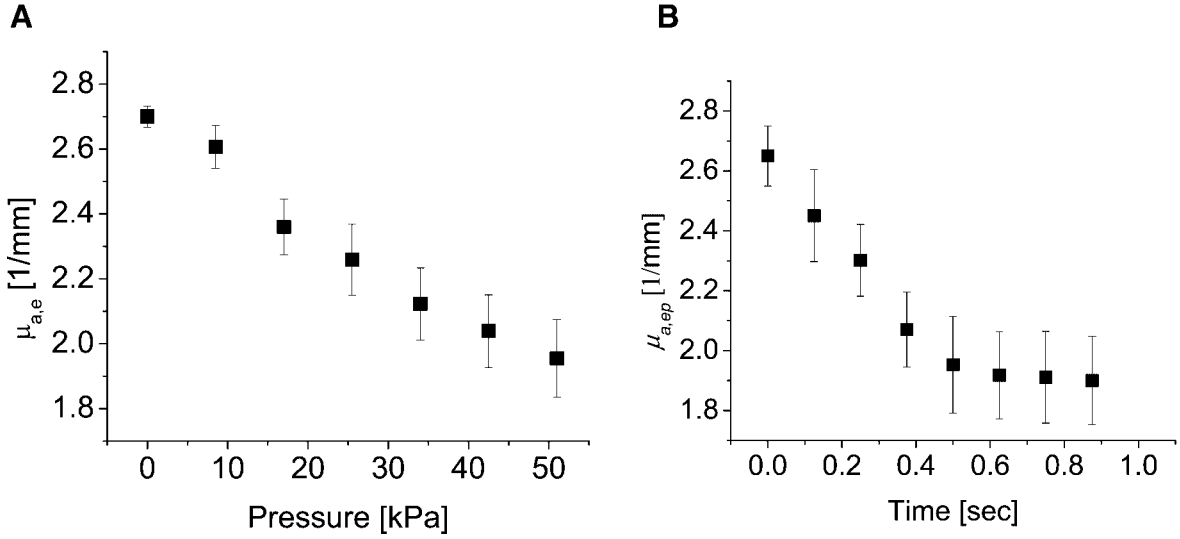

Fig. 11. VRS results: (**A**) change in epidermal absorption at 585 nm as a function of applied P_v on the forearm of a 24-year-old male with type II skin; (**B**) change in epidermal absorption at 585 nm as a function of time with the application of $P_v = 50$ kP_a on the palm of a 24-year-old male with type II skin.

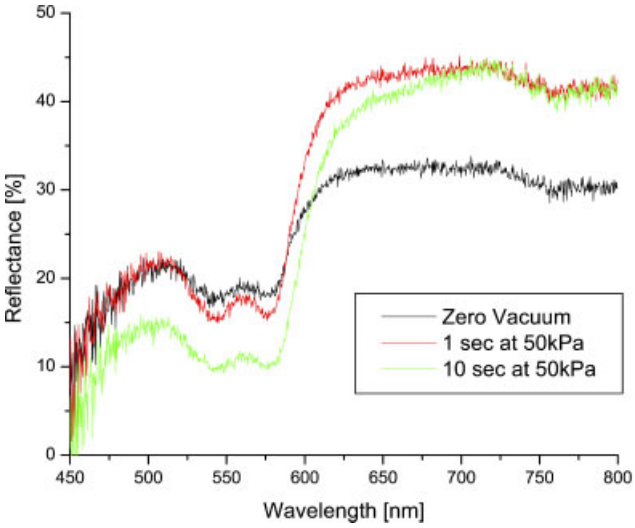

Fig. 12. Sample VRS measurements before and after 1 and 10 seconds of application of P_v.

decrease in the reflectivity over the entire spectrum is observed, also indicative of increase BVF, neither the characteristic oxyhemoglobin peaks or dips in this reflection representation. (542 and 577 nm) disappear, nor the oxyhemoglobin peak at 760 nm increases as seen in Svaasand et al. [10], suggesting that little or no effect of blood oxygenation is present during the application of P_v for up to 10 seconds.

CONCLUSIONS

Vacuum-assisted laser therapy has several major advantages over traditional treatment. It not only reduces epidermal absorption by thinning and stretching the skin surface, but also dilates blood vessels increasing the tissue BVF. This study suggests that the increase in BVF due to the application of P_v is not simply caused by mechanical interactions alone but is likely a result of a physiological response of the local microcirculation as well. The time required for bulk tissue to be displaced and the epidermal absorption coefficient to change due to the vacuum occurs within the first second of applied P_v, while the BVF and vessel diameter (D_v) for the same tissue can take up to 10 seconds to reach equilibrium. This time table for vessel dilation should be considered in the selection of the time sequence between the suction time and laser irradiation onset during clinical applications of vacuum-assisted laser therapy.

ACKNOWLEDGMENTS

The partial presentation of this work at the 2006 Annual Meeting of the American Society for Laser Medicine and Surgery was supported by a travel grant from the United States Air Force Office of Scientific Research to MC. We would like to thank Dr. Rong Zhang and Dr. John Viator for their technical guidance and support concerning the diffusion approximation model and spectrometer. We would also like to thank Kevin Chu for his help with carrying out the vacuum experiments.

REFERENCES

1. Chang CJ, Nelson JS. Cryogen spray cooling and higher fluence pulsed dye laser treatment improve port-wine stain clearance while minimizing epidermal damage. Dermatol Surg 1999;25(10):767–772.
2. Nelson JS, Milner TE, Anvari B, Tanenbaum BS, Kimel S, Svaasand LO, Jacques SL. Dynamic epidermal cooling during pulsed laser treatment of port-wine stain. A new methodology with preliminary clinical evaluation. Arch Dermatol 1995;131(6):695–700.
3. Nelson JS, Majaron B, Kelly KM. Active skin cooling in conjunction with laser dermatologic surgery. Semin Cutan Med Surg 2000;19(4):253–266.
4. Nelson JS, Milner TE, Anvari B, Tanenbaum BS, Svaasand LO, Kimel S. Dynamic epidermal cooling in conjunction with laser-induced photothermolysis of port wine stain blood vessels. Lasers Surg Med 1996;19(2):224–229.
5. Lanigan SW. Port-wine stains unresponsive to pulsed dye laser: Explanations and solutions. Br J Dermatol 1998; 139(2):173–177.
6. Fiskerstrand EJ, Dalaker M, Norvang LT. Laser treatment of port wine stains: A study comparing therapeutic outcome with morphologic characteristics of the lesions. Preliminary results. Acta Derm Venereol 1995;75(1):92–93.
7. Sivarajan V, Mackay IR. The depth measuring videomicroscope (DMV): A non-invasive tool for the assessment of capillary vascular malformations. Lasers Surg Med 2004; 34(2):193–197.
8. Sivarajan V, Mackay IR. Noninvasive in vivo assessment of vessel characteristics in capillary vascular malformations exposed to five pulsed dye laser treatments. Plast Reconstr Surg 2005;115(5):1245–1252.
9. Franco W, Childers M, Stuart Nelson J, Aguilar G. Laser surgery of port wine stains using vacuum pressure: Changes in calculated energy deposition (part II). Lasers Surg Med 2007;39(2):118–127.
10. Svaasand LO, Aguilar G, Viator JA, Randeberg LL, Kimel S, Nelson JS. Increase of dermal blood volume fraction reduces the threshold for laser-induced purpura: Implications for port wine stain laser treatment. Lasers Surg Med 2004;34:182–188.
11. Aguilar G, Svaasand LO, Nelson JS. Effects of hypobaric pressure on human skin: Feasibility study for port wine stain laser therapy (part I). Lasers Surg Med 2005;36(2):124–129.
12. Viator JA, Komadina J, Svaasand LO, Aguilar G, Choi B, Stuart Nelson J. A comparative study of photoacoustic and reflectance methods for determination of epidermal melanin content. J Invest Dermatol 2004;122(6):1432–1439.
13. Duck FA, Physical, properties of tissue. San Diego: Academic Press Inc.; 1990.
14. Skalak R, Chien S. Handbook of bioengineering. New York: Mcgraw-Hill Book Company; 1987.
15. Hendriks FM. Mechanical behaviour of human epidermal and dermal layers in vivo. Eindhoven: Technische Universiteit Eindhoven; 2005.
16. Lees C, Vincent JF, Hillerton JE. Poisson's ratio in skin. Biomed Mater Eng 1991;1(1):19–23.
17. Ophir J, Alam SK, Garra BS, Kallel F, Konofagou EE, Krousko T, Merritt CRB, Rrghett R, Souchon R, Srinivasan S, Varghese T, Elastography: Imaging the elastic properties of soft tissues with ultrasound. Med Ultrasonics 2002; 29(Winter):155–171.
18. Berardesca E, Andersen PH, Bjerring P, Maibach HI. Erythema induced by organic solvents: In vivo evaluation of oxygenized and deoxygenized haemoglobin by reflectance spectroscopy. Contact Dermat 1992;27(1):8–11.
19. Saidi IS, Jacques SL, Tittel FK. Mie and Rayleigh modeling of visible-light scattering in neonatal skin. Appl Opt 1995; 34(31):7410–7418.

20. Meglinski IV, Matcher SJ. Quantitative assessment of skin layers absorption and skin reflectance spectra simulation in the visible and near-infrared spectral regions. Physiol Meas 2002;23:741–753.
21. Svaasand LO, Norvang LT, Fiskerstrand EJ, Stopps EKS, Berns MW, Nelson JS. Tissue parameters determining the visual appearance of normal skin and port-wine stains. Lasers Med Sci 1995;10(1):55–65.
22. Douven LF, Hollinger JO, Jacques SL, Lucassen GW. Retrieval of optical properties of skin from measurement and modeling the diffuse reflectance. Proc SPIE 2000;3914: 312–323.
23. Zhang R, Verkruysse W, Choi B, Viator JA, Jung R, Svaasand LO, Aguilar G, Nelson JS. Determination of human skin optical properties from spectrophotometric measurements based on optimization by genetic algorithms. J Biomed Opt 2005;10(2):024030-I–024030-II.
24. Hendriks FM, Brokken D, van Eemeren JT, Oomens CW, Baaijens FP, Horsten JB. A numerical-experimental method to characterize the non-linear mechanical behaviour of human skin. Skin Res Technol 2003;9(3):274–283.
25. Guzelsu N, Federici JF, Lim HC, Chauhdry HR, Ritter AB, Findley T. Measurement of skin stretch via light reflection. J Biomed Opt 2003;8(1):80–86.
26. Costanzo LS. Physiology. 3rd ed. Saunders/Elsevier; 2003.
27. Ganong WF. Review of Medical Physiology, Stamford, Connecticut: Appleton and Lance 1997.
28. Tuchin VV. Optical clearing of tissues and blood, Bellingham, WA: The International Society for Optical Engineering; 2005.
29. Jacques SL, Narukar VA, Anderson R. The optics of stretching skin and use during clinical laser treatments: Oregon Health and Science University, Bay Area Laser Institute, Aesthera Corporation; 2005.
30. Chan EK, Sorg B, Protsenko D, ONeil M Motamedi M, Welch AJ. Effects of compression on soft tissue optical properties. IEEE J Selected Top Quantum Electron 1996; 2(4):943–950.